Strategies for laser-induced fluorescence detection of nitric oxide in high-pressure flames. III. Comparison of *A–X* excitation schemes

Wolfgang G. Bessler, Christof Schulz, Tonghun Lee, Jay B. Jeffries, and Ronald K. Hanson

Laser-induced fluorescence (LIF) has proven a reliable technique for nitric oxide (NO) diagnostics in practical combustion systems. However, a wide variety of different excitation and detection strategies are proposed in the literature without giving clear guidelines of which strategies to use for a particular diagnostic situation. We give a brief review of the high-pressure NO LIF diagnostics literature and compare strategies for exciting selected transitions in the *A–X*(0, 0), (0, 1), and (0, 2) bands using a different detection bandpass. The strategies are compared in terms of NO LIF signal strength, attenuation of laser and signal light in the hot combustion gases, signal selectivity against LIF interference from O_2 and CO_2, and temperature and pressure sensitivity of the LIF signal. The discussion is based on spectroscopic measurements in laminar premixed methane–air flames at pressures between 1 and 60 bars and on NO and O_2 LIF spectral simulations.

OCIS codes: 280.1740, 300.2530.

1. Introduction

Laser-induced fluorescence (LIF) is an important tool[1–3] to help understand nitric oxide (NO) formation in both practical combustion systems and laboratory flames. Investigations aim to develop engineering solutions to minimize NO effluent, as well as to develop and validate chemical kinetic models of NO formation and destruction. The high operating pressure of practical combustors [internal combustion (IC) engines, gas turbines] requires strategies for quantitative NO LIF measurements at pressures exceeding 50 bar.

Different approaches for NO excitation have been previously suggested, including NO excitation in the *D–X*(0, 1) band and in several *A–X* vibrational bands, without, however, giving clear guidelines as to the transitions favorable in a given diagnostic situation. This paper is the third in a series of papers where we compare excitation strategies in the *A–X* band to evaluate strategies for LIF at elevated pressures. In the previous papers we investigated different excitation strategies within single vibrational levels [NO *A–X*(0, 0)[4] and *A–X*(0, 1)[5]] and provided recommendations for specific NO excitation features within these bands. In earlier papers we focused on *A–X*(0, 2) excitation.[6,7] Our aim in this paper is to compare the best strategies found in the previous papers to provide guidelines for the optimum excitation and detection strategies for NO LIF in specific combustion situations and pressures. The comparison takes into account the influences of signal strength, laser and signal transmission, signal interference, and pressure and temperature dependence. The discussion is based on spectrally resolved NO LIF measurements in premixed methane–air flames at 1–60 bar and on NO and O_2 spectral simulations.

2. Background

A. Interpretation and Quantification of NO Laser-Induced Fluorescence Signals

The conversion of measured NO LIF intensities to relative NO concentrations requires correction for the influence of temperature, pressure, and the concentrations of all other species, as well as the knowledge of the influence of these factors on the NO spectros-

The authors are with the High Temperature Gasdynamics Laboratory, Department of Mechanical Engineering, Stanford University, Stanford, California 94305-3032. The permanent address for W. G. Bessler and C. Schulz is Physikalisch-Chemisches Institut, Ruprecht-Karls-Universität Heidelberg, Im Neuenheimer Feld 253, Heidelberg 69120, Germany. The e-mail address for J. B. Jeffries is jay.jeffries@stanford.edu.

Received 21 January 2003; revised manuscript received 16 May 2003.

0003-6935/03/244922-15$15.00/0

copy.[2] We refer to such corrected LIF intensities as semiquantitative NO concentrations. Furthermore, calibration of the corrected LIF intensities to absolute number densities or mole fractions is required for quantitative NO concentration measurements, accounting for the influence of collection optics, detector quantum efficiency, and laser energy density.

The main temperature influence of the NO LIF signal strength arises from the ground-state population of the laser-coupled levels. Furthermore, temperature, pressure, and gas phase composition affect the frequency and cross section of collisions that a NO molecule encounters. This influences both the excitation efficiency by altering the shape of the absorption spectra and the fluorescence quantum yield. Collisional (pressure) broadening and line shifting have been measured for the NO *A–X* band for collisions with the main combustion species.[8–11] Variations in pressure, temperature, and (less importantly) gas phase composition influence the spectral overlap of the laser line profile with the NO absorption features. As a result, excitation efficiency and therefore the LIF signal decrease with increasing pressure. Collisional fluorescence quenching of the NO *A* state has been investigated in detail,[12–15] and models have been established and validated to describe the effects of temperature and colliding species on quenching cross sections.[16–18] The quenching rate scales directly with pressure. Because quenching is the dominant depopulation path of the NO *A* state, the fluorescence quantum yield and therefore the LIF signal decrease strongly with increasing pressure and further vary with temperature and gas composition.

Pressure can be measured accurately in most situations and with high temporal resolution by use of piezoelectric sensors, and the correction of the LIF signals for pressure is therefore quite feasible. The measurement of temperature, on the other hand, requires a large experimental effort, and it is usually not feasible to obtain temperature information simultaneously for NO LIF data in practical, often turbulent, applications. Modeled temperatures can be used to correct NO LIF intensities; however, the accuracy is severely limited in unsteady flames. Thus quantitative NO concentration measurements without the exact knowledge of local temperature often require the choice of a transition that minimizes the total temperature sensitivity of the LIF signal. This does not necessarily mean that one has to choose a level with a population with minimum temperature sensitivity. In some cases a systematic variation of the ground-state population with temperature might be desired to compensate for other temperature-dependent effects.

Even less available than temperature is the concentration of colliding species. Although chemical simulations are feasible in laminar flames and multispecies Raman measurements[19] can provide the required information for point or line measurements, NO LIF imaging in turbulent combustion situations normally cannot be corrected for composition fluctuations. The introduced error, however, is relatively small for premixed combustion because NO is present only in the post-flame-front gases where the majority species concentrations are known relatively precisely.

B. Motivation for Different *A–X* Excitation Strategies: Transmission Properties

Excitation within the *A–X*(0, 0) band is the established standard technique for LIF diagnostics of NO (see Subsection 2.D). However, the relatively short laser wavelengths involved (around 225 nm) are strongly absorbed in high-temperature, high-pressure combustion environments. Recently it was recognized that the main absorbing species are hot CO_2 and H_2O present in the combustion gases. UV light at short wavelengths (<250 nm) is strongly absorbed by these species,[20] and absorption cross sections increase with temperature and decrease with wavelength.[21] The effect increases with pressure because of the increasing number density of absorbers, leading to strong attenuation of both laser and signal light even in small-flame geometries.[22,23]

These observations made clear that excitation at longer wavelengths is desirable. They motivated a comparison of the conventional *A–X*(0, 0) excitation with strategies exciting transitions within the *A–X*(0, 1) (around 236 nm) and the *A–X*(0, 2) (around 247 nm) bands. Because excitation within the (0, 0), (0, 1), and (0, 2) all populate the same excited vibrational level ($v' = 0$), quenching and excited-state energy-transfer processes and therefore signal interpretation are similar for these approaches. However, a careful consideration of signal interference and temperature dependence is necessary to assess the feasibility of these different approaches.

C. Signal Strength and Signal Interference

LIF measurements of NO are faced with difficulties in selectivity. This is true especially in high-pressure combustion environments, where laser-induced emission not only from NO but also from other species present in the flame becomes important if not dominant. Use of an appropriate excitation wavelength and detection bandpass is crucial to maximize signal strength and minimize potential interference. This has been discussed in detail in our previous studies for selection of excitation wavelength in each individual vibrational band.[4,5] In this paper we compare the differences for exciting using the three vibrational bands. There are three primary sources of signal interference, and their influence depends on the specific combustion situation.

- O_2 LIF interference. Hot O_2 is the main contributor to LIF interference in lean and nonpremixed flames. The $B^3\Sigma^- – X^3\Sigma^+$ Schumann–Runge bands of O_2 overlap with the $A\ ^2\Sigma^+ – X\ ^2\Pi$ NO gamma bands over a wide range of excitation wavelengths[1] resulting in overlapping absorption features and fluorescence signals. Because the fluorescence lifetime of the relevant excited states of O_2 is limited by predis-

sociation, the pressure influence on line broadening and fluorescence quantum yield is much smaller than for NO. This leads to an increase of the relative contribution of O_2 LIF background with increasing pressure.[4] To avoid this interference problem with broadband LIF detection, a careful choice of excitation transition is necessary. Furthermore, different strategies have been suggested to correct for the remaining interference. For example, DiRosa *et al.* suggested broadband detection (230–290 nm) with subsequent subtraction of the O_2 LIF contribution measured simultaneously in another detection band (310–400 nm).[24] However, this approach has not yet been used for measurements in practical systems, mainly because the measurement of O_2 LIF without additional interference is not an easy task.

- CO_2 broadband LIF emission. The contribution of CO_2 LIF was recently identified in lean, stoichiometric, and rich high-pressure methane–air and methane–oxygen–argon flames.[25] This signal consists of a broad (200–450 nm) continuum with a faint superimposed band structure, and its fluorescence yield is constant for pressures up to at least 40 bar. Like with O_2, the relative influence of the CO_2 LIF increases with pressure as the NO fluorescence yield is proportional to 1/p. Although the signal is comparatively weak, it can become an important contribution to the overall signal when detection over wide spectral ranges is used.
- Polycyclic aromatic hydrocarbon (PAH) LIF interference in rich flames. In rich and nonpremixed flames additional broadband fluorescence interference has been observed that is usually attributed to PAHs and partially burned hydrocarbons (aldehydes, ketones).[26] In sooting flames at high laser energies, interference by LIF of laser-generated C_2 has also been reported.[27] Laser-induced incandescence is observed in sooting flames,[28] however at considerably longer wavelengths (>350 nm) than normally used for NO detection (<300 nm). The research reported here concentrates on premixed flames with the equivalence ratio $\phi < 1.2$ where the PAH interference is relatively minor. Research on CO_2 LIF shows the onset of strong PAH interference near $\phi = 1.6$.

An appropriate choice of the NO LIF signal detection wavelength is most important for the discrimination against interfering signals. With A–X(0, 0) excitation, detection is possible only at longer wavelengths (red shifted) relative to the excitation wavelengths. Excitation within the A–X(0, 1) and (0, 2) bands offers the possibility for blue-shifted detection, leading to more effective suppression of CO_2 and PAH LIF signals that occur almost exclusively red shifted relative to the excitation wavelength.

D. Literature Review

A large number of NO LIF measurements have been performed in high-pressure flames with both D–X and A–X strategies. In this subsection we give a brief review of that research. We focus on elevated pressure combustion, but some atmospheric-pressure studies are also cited where appropriate.

1. D–X(0, 1) Excitation

The NO D–X(0, 1) system at 192–195 nm can be probed with 193-nm radiation from an ArF excimer laser.[29,30] Andresen *et al.*[31] applied this approach for qualitative NO LIF imaging in a spark-ignition gasoline engine fueled with isooctane. Arnold *et al.*[32,33] carried out measurements in a direct-injected (DI) Diesel engine fueled with n-heptane. Ter Meulen and co-workers showed NO imaging in a prechamber-injected Diesel engine fueled with n-heptane and Diesel fuel.[34,35] They subsequently performed measurements in a DI Diesel engine with maximum pressures of 75 bar.[36,37] Tanaka *et al.* performed measurements in a spark-ignition engine.[38] In most of the research, the ArF excimer laser was tuned to the D–X(0, 1) $R_1(26.5) + Q_1(32.5)$ transition at 193.38 nm with subsequent detection of D–X(0, 3) emission around 208 nm. This transition was shown earlier to minimize O_2 LIF interference.

The major drawback of the D–X excitation approach is the severe attenuation of the short-wavelength laser beam and signal light in the high-pressure combustion atmosphere, leading to complete signal loss over portions of the engine cycle and disabling the quantitative interpretation of the signal. Andersen *et al.*[31] reported complete laser absorption in the cylinder after ignition to crank angles as late as 150 deg after top dead center, when pressure has dropped from the maximum of 30 bar to below approximately 5 bar. Stoffels *et al.*[37] observed transmissions of 0–1.2% through the 82-mm-diameter cylinder for all investigated crank angles between −20 and 100 deg relative to top dead center. Techniques that were developed to correct for the laser attenuation[35] are based the questionable assumption that attenuation is caused by light scattering only.

Interpretation of the LIF signals is further complicated by the fact that little is known about quenching and electronic energy-transfer processes of the NO D state. Attempts for absolute interpretation[36,37] must rely on unverified assumptions about the dependence of fluorescence quantum yield on pressure and temperature.

2. A–X(0, 0) Excitation

The largest number of NO LIF measurements that were performed in low-, atmospheric-, and high-pressure flames use A–X(0, 0) excitation at 224–227 nm. It is thus the standard technique for NO detection in flames, and it is the only technique sensitive to cold NO, e.g., in flow-field diagnostics.[39,40] High-pressure applications include small-scale laboratory flames and gasoline and Diesel IC engines with different signal collection strategies varying from narrowband detection [3-nm bandpass detecting A–X(0, 1) emission[41]] to broadband detection integrating over several vibrational bands [for example, Dec and Canaan: A–X(0, 1) to (0, 4)[42]].

Alatas *et al.*[43] performed the first in-cylinder measurements with A–$X(0, 0)$ excitation to our knowledge. They showed qualitative NO LIF images in a direct-injection Diesel engine. Unfortunately they did not give any details about the excitation and detection wavelengths used, which makes it hard to judge the level of selectivity they reached.

Bräumer *et al.* used the $R_1+Q_{21}(21.5)$ transition at 225.25 nm for quantitative in-cylinder NO number density measurements in a spark-ignition engine fueled with propane.[44] The transition was chosen on the basis of the available laser source: The 248-nm output of a tunable narrowband KrF excimer laser was shifted to its first anti-Stokes wavelength at 226 nm in a 10-bar hydrogen cell[45]; this approach yielded sufficient laser energy (several millijoules) for imaging measurements.

Dec and Canaan[42] performed imaging measurements in a DI Diesel engine fueled with low-sooting Diesel fuel. They used average LIF intensity images to derive semiquantitative in-cylinder NO concentrations throughout the combustion cycle with pressures up to 65 bar. A frequency-doubled optical parametric oscillator system was used to excite the $P_1(23.5)$, $Q_1+P_{21}(14.5)$, $Q_2+R_{12}(20.5)$ feature at 226.03 nm. This transition was proposed by Battles and Hanson[46] based on detailed spectroscopic investigations and studied in flames up to 10 bar by DiRosa *et al.*[24] Van den Boom *et al.* used the same transition in a DI Diesel engine fueled with commercial Diesel.[47] Nakagawa *et al.* used 226.29-nm excitation in Diesel spray flames in a modified single-cylinder engine.[48]

A large number of NO measurements were presented in high-pressure laboratory burners. Laurendeau and co-workers studied NO formation in premixed, partially premixed, and nonpremixed flames. They showed quantitative NO point measurements in ethane–air flames up to 15 bar,[49–52] ethylene–air flames up to 12 bar,[53] methane–air flames up to 15 bar,[41] heptane spray flames at 2–5 bar,[54–56] and $CO/H_2/CH_4$/air flames at 1–12 bar.[57] For most of the measurements, they tuned their frequency-doubled dye laser system to the $Q_2(26.5)$ transition at 225.58 nm. This transition was chosen to minimize temperature dependence of the ground-state population. Spectroscopic measurements in the 1–15-bar range were carried out to investigate O_2 LIF interference,[58,59] and the influence of pressure on calibration was investigated.[60] Narrowband monochromator detection (<5-nm bandpass) was used in most of the research for effective interference suppression; however, significant interference was observed with broadband imaging detection in the 4-bar spray flame.[55,61]

In previous research, we investigated different transitions within the A–$X(0, 0)$ band in detail in premixed flat CH_4–air flames up to 60 bar and discussed their applicability for high-pressure combustion situations.[4] It was shown that the transition originally proposed by DiRosa *et al.*[24] is clearly superior to other approaches in terms of both signal strength and suppression of O_2 LIF interference. This transition was used for quantitative temperature and NO concentration imaging in high-pressure flames.[22,62] Temperature measurements with NO LIF were also performed by Vyrodov *et al.* in rich premixed methane–air flames up to 30 bar.[63]

Several authors reported strong attenuation of the 226-nm laser beam in engines, making in-cylinder measurements impossible at crank angles around top dead center.[43,47] In earlier measurements, we reported laser and signal absorption of nearly 45% at 60 bar despite the small size (8-mm diameter) of our laboratory flame.[22] Thus absorption is of big concern with A–$X(0, 0)$ excitation and motivates the investigation of excitation in longer-wavelength vibrational bands.

3. A–$X(0, 1)$ Excitation

Application of NO A–$X(0, 1)$ excitation in the 233–237-nm wavelength range is promising because it reduces laser beam attenuation [which is a problem with D–X and A–$X(0, 0)$ excitation] while still providing strong signals [which is a problem with A–$X(0, 2)$ excitation]. Furthermore, optical parametric oscillator systems provide high laser-pulse energies throughout the UV (up to 30 mJ) that is needed for imaging measurements.

To our knowledge, the first application of NO A–$X(0, 1)$ LIF in high-pressure combustion was performed by Jamette *et al.* in a DI spark-ignition gasoline engine.[64] These authors chose the $R_1+Q_{21}(22.5)$, $Q_1+P_{21}(8.5)$, $Q_2+R_{12}(17.5)$ feature at 236.22 nm based on simulations of LIF excitation spectra of NO and O_2 to maximize the NO/O_2 LIF ratio However, no experimental spectroscopic data were available to support this choice. Signals were detected within the A–$X(0, 2)$ band.

We performed detailed investigations of three different A–$X(0, 1)$ excitation schemes in premixed flat methane–air flames up to 60 bar.[5,65,66] Although the scheme used by Jamette *et al.* showed best performance in terms of signal strength, reduced O_2 LIF interference in lean flames was found with $P_1(25.5)$, $R_1+Q_{21}(11.5)$, $Q_1+P_{21}(17.5)$ excitation at 235.87 nm.

4. A–$X(0, 2)$ Excitation

A–$X(0, 2)$ excitation at 244–247 nm is popular because of the availability of strong KrF excimer lasers providing appropriate wavelengths to excite the O_{12} bandhead at 247.94 nm. This approach was first proposed by Schulz *et al.*[67] to avoid the strong laser and signal attenuation observed with D–$X(0, 1)$ or A–$X(0, 0)$ excitation. They performed detailed spectroscopic investigations in premixed flat methane–air flames up to 40 bar[6,7,68] to assess interference from O_2 LIF and found that the NO A–$X(0, 2)$ O_{12} bandhead coincides with a local minimum in the O_2 B–X band. In addition, (0, 2) excitation offers the possibility of blue-shifted detection of the (0, 0) and (0, 1) emission, providing an important advantage by eliminating the detection of CO_2 and PAH LIF.[69] This scheme was also investigated in sooting high-pressure ethylene–

air flames[70] where strong PAH fluorescence is observed red shifted to the excitation wavelength but the blue-shifted NO detection minimizes this interference. The signal from the A–$X(0, 0)$ band can potentially be attenuated by fluorescence trapping if the signal travels through areas with high NO concentrations over long path lengths. However, even in engine experiments it was shown that this effect is negligible (<5%) compared with light attenuation by hot combustion products (CO_2).[71]

Schulz and co-workers applied this scheme for quantitative NO concentration imaging in a spark-ignition engine fueled with propane.[72] Simultaneous Rayleigh temperature measurements were performed and used to quantify the NO LIF images. Quantitative imaging measurements were also performed in spark-ignition engines fueled with isooctane running under premixed and nonpremixed (DI)[69,73] conditions and in DI Diesel engines fueled with commercial Diesel fuel.[74,75]

The A–$X(0, 2)$ approach was proposed independently by Andresen and co-workers. They performed spectroscopic investigations on NO LIF with A–$X(0, 2)$ excitation in an atmospheric-pressure flame, measured transmission properties in a spark-ignition engine fueled with isooctane, and showed qualitative NO LIF distributions in that engine.[76,77] Quantitative one-dimensional measurements were shown in a spark-ignition engine fueled with isooctane and regular gasoline.[78] The spectrograph detection used in these measurements enabled the assessment of Raman and LIF interferences as well as investigation of fluorescence trapping.

Qualitative in-cylinder measurements with A–$X(0, 2)$ bandhead excitation have been performed by Akihama *et al.* in a port-fuel-injected spark-ignition engine fueled with isooctane at pressures up to 15 bar.[79]

3. Experiment

A. High-Pressure Burner

The experimental setup is identical to the ones previously used.[4,5] Laminar, premixed methane–air flat flames at pressures from 1 to 60 bar were stabilized on a porous, sintered stainless-steel plate of 8 mm in diameter; this burner was mounted in a stainless-steel housing with an inner diameter of 60 mm with a pressure stabilization of ±0.1 bar.[80] Investigations were performed for fuel/air equivalence ratios of $\phi = 0.83, 0.93, 1.03$, and 1.13. All measurements were carried out with 300-parts per million (ppm) NO seeded to the feedstock gases to mimic enginelike conditions. Optical access to the flame was possible through four quartz windows (Fig. 1). A Nd:YAG-pumped (Quanta Ray GCR250) frequency-doubled (β-barium borate) dye laser (LAS, LDL205) produced laser light [approximately 1-mJ, 0.4-cm^{-1} full width at half-maximum (FWHM)] at 224–227 nm for NO A–$X(0, 0)$ excitation (Coumarin 120 dye),[4] 233–238 nm for A–$X(0, 1)$ excitation (Coumarin 102 dye),[5] and 245–248 nm for A–$X(0, 2)$ excitation (Coumarin 307 dye). The laser beam was aligned parallel to the burner surface and passed through the center of the flame 2 mm above the burner matrix. The beam was focused with lenses into the flame. The pulse energy was measured with a photodiode (LaVision). Fluorescence signals were collected at right angles to the laser beam and line imaged with a $f = 105$ mm, f-number = 4.5 achromatic UV lens (Nikon) onto the horizontal entrance slit of a 250-mm imaging spectrometer (Chromex 250IS) equipped with a 600-grooves/mm grating. The dispersed fluorescence signals were detected with an intensified CCD camera (LaVision FlameStar III). Each laser pulse yielded a complete fluorescence spectrum maintaining one-dimensional spatial resolution along the laser light path. In these images the central area of the flame where temperature and concentrations are homogeneous was then chosen and integrated over the spatial axis, yielding a fluorescence spectrum.

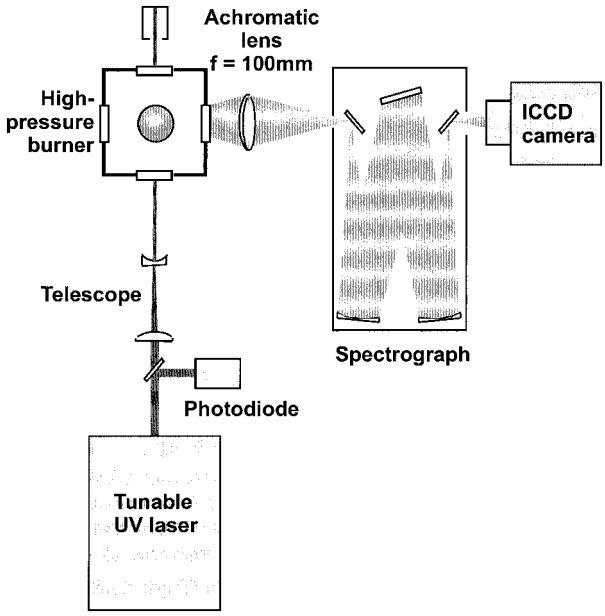

Fig. 1. Experimental arrangement with the laser line aligned along the spectrometer slit. ICCD, intensified CCD.

The laser was tuned to record excitation spectra in a ±0.0125-nm range around specific NO transitions within the A–X bands. The transitions investigated in each band are summarized in Table 1. Their choice is based on previous results and simulation calculations as described in Refs. 4 and 5. The signal was averaged over 20–50 laser pulses for each excitation wavelength and stored for further evaluation before the laser was scanned to the next wavelength. The applied laser fluences (<35 MW/cm^2) are in the range of linear LIF laser excitation for pressures above 5 bar.[7] This corresponds to the relevant pressure range for comparison of NO LIF with interference signals (interference signal strengths were below the detection limit for $p < 5$ bar throughout the complete set of measurements). The spectra were therefore linearly corrected for variations in laser-pulse energy.

Table 1. Spectroscopic Data of the Transitions Used in the NO *A–X* Bands

A–X Band	Transition	Excitation Wavelength (nm)	Ground-State Energy ε/κ (K)
(0, 0)	$P_1(23.5)$, $Q_1 + P_{21}(14.5)$, $Q_2 + R_{12}(20.5)$	226.03	540–1381
(0, 1)	$P_1(25.5)$, $R_1 + Q_{21}(11.5)$, $Q_1 + P_{21}(17.5)$	235.87	3040–4305
(0, 2)	$O_{12}(7.5–10.5)$ bandhead	247.94	5680–5820

B. Assessment of Interference Signals

The emission spectra at excitation wavelengths corresponding to maximum NO LIF intensities were evaluated to separate and quantify the overlapping LIF signals of NO, O_2, and CO_2. Raman signals were not observed in the hot flame gases (the laser was polarized horizontally for maximum suppression of the Raman signal). The experimental data were corrected for the wavelength-dependent detection efficiency and signal absorption from hot exhaust gases.[21] A nonlinear least-squares fitting procedure was used to separate the various overlapping LIF spectra and the contribution of elastically scattered light (Rayleigh) and to account for the (Voigt-type) spectrograph slit function (as obtained from fits to measured spectra). The intensities of simulated NO and O_2 LIF emission spectra,[81] experimental CO_2 LIF emission spectra,[25] and a Rayleigh signal were simultaneously fitted to the experimental data. The O_2 LIF emission spectra are complex because of overlapping absorption lines leading to simultaneous excitation into multiple vibrational states. Furthermore, vibrational energy transfer in the upper electronic (B) state was evident from the O_2 LIF emission structure. Therefore emission signals from multiple upper vibrational O_2 B states were fitted independently.

We reevaluated the A–$X(0, 0)$ and (0, 1) data from our previous studies[4,5] using this more sophisticated fitting technique and incorporating new data on CO_2 fluorescence.[25] Compared with the previous approach (based on Gaussian fits only), the new technique (based on simulated spectra) allows larger spectral regions to be fit and therefore yields information about the contribution of broadband signals. In addition, we investigated A–$X(0, 2)$ O_{12} bandhead excitation at 247.94 nm. The overall fit reproduces the experimental data well. Figure 2 shows emission spectra and fitting results for the excitation strategies compared in this paper for lean 60-bar flames.

C. Quantification of NO Laser-Induced Fluorescence Signals

Despite constant NO seeding (300 ppm in the fresh gases), the actual NO concentrations decrease in rich flames because of NO reburn chemistry. More precisely, the NO concentration in the flame equals the natural NO concentration (without NO seeding) plus the NO seeding concentration multiplied by an equivalence-ratio-dependent reburn factor. Furthermore, the NO LIF signal yield depends on temperature, pressure, and the equivalence ratio. Thus the ratio of the NO LIF signal to the background signal is biased for different flame conditions. To enable an accurate comparison for different flames (pressure, equivalence ratio), the following quantification procedure is applied to calculate LIF signal intensities for a constant NO concentration of 300 ppm in all flames.

The NO LIF signal strength measured in the $\phi = 0.93$ flames is quantified by the temperature and concentration data of our previous research.[22] Reburn is known to be minimal for these slightly lean conditions, and a 10% reburn of the seeded NO is assumed.[82] From the derived NO concentration value at $\phi = 0.93$, the expected LIF signal intensities of

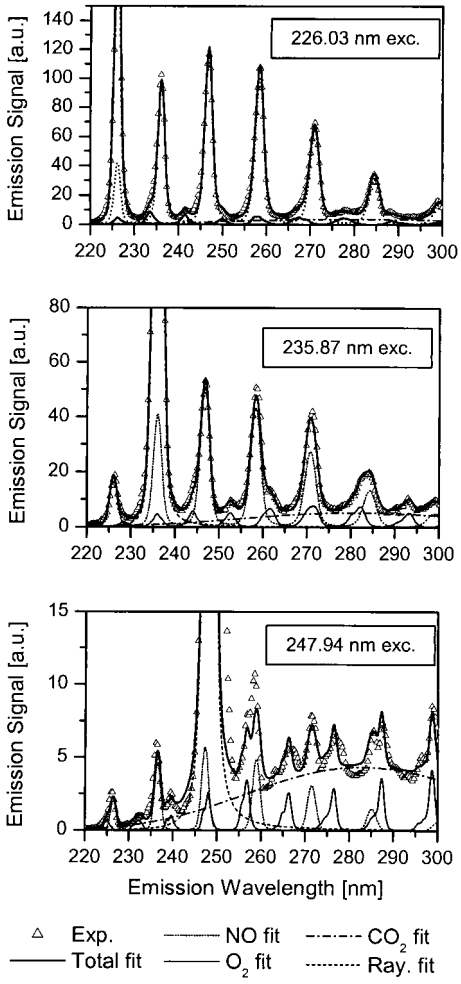

Fig. 2. Examples of the nonlinear least-squares fit of simulated NO, O_2, CO_2, and Rayleigh (Ray.) emission spectra (represented as Voigt line shapes) for the investigated excitation (exc.) strategies at $p = 60$ bar, $\phi = 0.83$. The arbitrary intensity units are the same in all panels. See text for details.

Table 2. Results of the Analysis for the Different Excitation and Detection Strategies: Comparison of Signal Strengths

NO *A–X* Band	(0, 0) Excitation (0, 1) + (0, 2) Detection	(0, 1) Excitation (0, 0) Detection	(0, 1) Excitation (0, 2) + (0, 3) Detection	(0, 2) Excitation (0, 0) + (0, 1) Detection	(0, 2) Excitation (0, 3) + (0, 4) Detection
	Excitation and Detection Strategy (nm)				
1-bar excitation wavelength	226.031	235.870	235.870	247.941	247.941
Detection bandpass	232–252	217–232	243–263	220–240	255–275
	Relative Signal Strengths at 10 bar (60 bar)				
Experimental, $\phi = 0.83$	100 (100)	18 (17)	42 (39)	4.1 (3.4)	2.3 (1.9)
Simulated, $T = 1900$ K	100 (100)	15 (14)	28 (26)	3.1 (3.1)	1.3 (1.4)

300-ppm NO are calculated for $\phi = 0.83$, 0.93, 1.03, and 1.13. In these calculations, we consider the variation of the quenching rate using calculations of equilibrium exhaust gas compositions, and an invariant flame temperature is assumed for the investigated range of equivalence ratios. Temperature-dependent quenching cross sections are calculated on the basis of published data.[16,18] The calculations are performed individually for each investigated pressure. We can therefore compare the O_2 and CO_2 background signal strengths with the LIF signal of 300-ppm NO for our flame conditions.

4. Comparison of *A–X* Strategies

The choice of a NO LIF detection strategy is governed by the combined effects of NO spectroscopy (signal strength, signal interference, pressure and temperature dependence, saturation), experimental setup (availability of laser source, detection system), measurement conditions (fixed or varying pressure, scale), and aim of the measurement (qualitative or quantitative, imaging or point measurements). The optimization of all these factors does not lead to a single excitation and detection strategy, but instead provides guidelines for the careful choice needed for any given diagnostic situation. The following discussion focuses on high-pressure combustion, but the same trends are true for atmospheric- or low-pressure flames, or reactive or nonreactive flows.

We compare one excitation strategy within each of the *A–X*(0, 0), (0, 1), and (0, 2) bands that was shown previously to yield best performance in terms of signal strength and interference suppression.[4–6] The particular transitions and their spectroscopic data are summarized in Table 1. For each excitation scheme, different detection strategies relevant for bandpass-filtered imaging in practical application are compared. With (0, 0) excitation only red-shifted detection is possible, but for (0, 1) and (0, 2) excitation we compare both red- and blue-shifted detection. In particular, we simulate 20-nm bandpass detection of two NO vibrational emission bands [except for blue-shifted detection after (0, 1) excitation where only one band can be detected]. The details for these five strategies are given in Table 2.

Usually, bandpass detection of the LIF signal is performed, acquiring the emission of one or more vibrational emission bands. The signal strength can easily be increased by detection of multiple bands (usually at the cost of increased interference). In many high-pressure burner applications, on the other hand, point measurements with narrowband monochromator detection were performed (see sub section 2.D). This strategy yields better signal/interference ratios, however at the cost of signal strength. When complete emission spectra are recorded (e.g., by use of an imaging spectrograph like the one used in this study), the selectivity can be further enhanced by fitting the different contributions of interfering species to the spectra prior to evaluating the NO LIF intensity. A comparison of these strategies is not attempted in this paper. The number of parameters that allows the optimization in a given situation is too large for a discussion of useful typical cases. Our data set, however, allows to us evaluate either of these strategies.

A. Signal Strength in Nonabsorbing Environments

To maximize signal strength, a NO transition with a large ground-state population at flame temperatures and high oscillator strength should be chosen. At typical combustion temperatures of 1500–2500 K, the largest vibrational population is present in the X $v'' = 0$ state. The $v'' = 1$ and 2 states have respective energies of 1846 and 3724 cm^{-1} above the ground state,[83] corresponding to maximum populations at ~2700 and ~5400 K, respectively. The largest lower-state populations are therefore found in the *A–X*(0, 0) band in most combustion applications. Slightly higher oscillator strengths of the (0, 1) and (0, 2) bands [factor of 1.4 and 1.1 higher than the (0, 0) strength, respectively] cannot compensate for the lower population. Because NO LIF involves excitation with narrow-bandwidth lasers, not only the vibrational strength but the strength of the particular rovibrational transition is relevant. Furthermore, absorption features consisting of multiple transitions (e.g., bandheads) can easily be found in the NO spectra and yield stronger signals than single transitions for pressures up to approximately 40 bar (before pressure broadening becomes dominant).

In high-pressure systems, where line broadening and shifting severely influence the excitation efficiency, an optimized strategy for NO LIF should involve excitation at a wavelength yielding maximum signal strength for each individual pressure. Be-

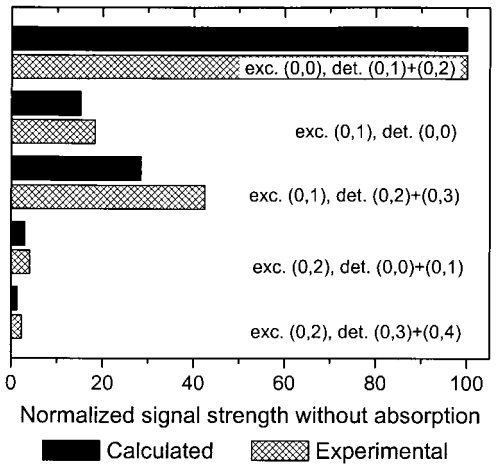

Fig. 3. Calculated and experimental signal strengths for the 10-bar flame for the excited (exc.) and detected (det.) vibrational bands within the NO A–X system.

cause the pressure shift is in the range of 0.2 cm^{-1}/bar,[8–11] this means that we tune the laser by several wave numbers in typical pressure ranges of 10–50 bar when exciting at the maximum of a single, isolated transition. In practical applications, however, pressure often varies rapidly (e.g., in IC engines). Here, a fixed excitation wavelength must be chosen. The resulting signal loss is most pronounced for pressures between 1 and 5 bar because of the simultaneous action of pressure broadening and shift. This effect can partly be reduced when broad, multiline absorption features are chosen.[4] In this paper, we acquired all results shown with the laser tuned to yield maximum NO LIF signals for each individual pressure.

Figure 3 shows measured and simulated signal strengths for the different A–X strategies for excitation in a 10-bar flame, normalized to the signal strength of the (0, 0) approach. The results are summarized in Table 2 that also gives the data for 60-bar flames. The simulations have been performed for a typical flame temperature of 1900 K.[22] The measurements in the different vibrational bands were carried out with different dye laser configurations over a period of several months. The comparison between these different schemes is therefore possible only within an estimated ±25% accuracy. Within this range, the experimental and simulated signal strengths agree well. The vibrational band strengths, however, are well known. Therefore there is no reason to doubt the relative intensities predicted by the simulations. A–X(0, 0) strategies clearly show the strongest signals; A–X(0, 1) excitation yields signal intensities approximately an order of magnitude lower. Signal is decreased by another order of magnitude with A–X(0, 2) excitation. The difference between red- and blue-shifted detection reflects the different Franck–Condon factors.

Considering signal strength alone, (0, 0) excitation is clearly the strategy of choice. However, in the hot postflame combustion gas where absorption coefficients are strongly wavelength dependent, the other strategies should not be discarded simply on the basis of signal strength. This is discussed in Subsection 4.B. Furthermore, the high laser power of the tunable excimer laser usually used for (0, 2) excitation may partially compensate for the low signal strength for imaging measurements where the output of dye lasers limits the excitation energy for the laser sheet.

B. Influence of Attenuation by Hot CO_2 and H_2O

Hot combustion products such as CO_2 and H_2O have long been ignored as potential absorbers in laser-based combustion diagnostics research. However, at wavelengths shorter than 250 nm for CO_2 and shorter than 230 nm for H_2O, their influence becomes relevant at flame temperatures and increases toward shorter wavelengths.[20,21] This causes attenuation of the laser as well as the fluorescence light. The transmission depends not only on the wavelength, but also on the path length and therefore on flame geometry and the experimental configuration. This produces nearly opposite effects: With (0, 0) excitation and red-shifted detection, strong laser attenuation with less signal attenuation occurs; with (0, 2) excitation and blue-shifted detection, laser attenuation is less but signal attenuation is stronger. For a quantitative comparison, laser and signal transmission are calculated for flame center positions in two typical high-pressure flame configurations: case 1, high-pressure burner, 40 bar, 1900 K, 8 mm in diameter (e.g., Ref. 22); case 2, DI Diesel engine, 50 bar, 2400 K, 80 mm in diameter, laser travels through cylinder window, detection is through piston window (e.g., Ref. 74).

The calculations are performed with the expressions given by Schulz *et al.*[23] for $\phi = 0.9$ equilibrium exhaust gas concentrations of CO_2 and H_2O. The results are given in Table 3. The different influence on laser and signal wavelengths can clearly be followed. In case 1, the high-pressure flame, total transmission (laser and signal) varies between 75 and 92% for the investigated strategies, and the difference between (0, 0) excitation/(0, 1),(0, 2) detection and (0, 2) excitation/(0, 0),(0, 1) detection is small (75 versus 82% total transmission). In case 2 for the Diesel engine, absorption is much stronger because of the higher temperatures and longer paths involved. In this geometry with a long laser path and a short signal path (detection through piston window), (0, 0) excitation has a strong disadvantage. In this case there is a large difference when comparing (0, 0) excitation/(0, 1),(0, 2) detection and (0, 2) excitation/(0, 0),(0, 1) detection, the latter strategy yielding a total transmission of 26 times that of the former.

Table 3 also gives relative signal strengths, normalized to the signal strength of the (0, 0) strategy without absorption. These data are also shown in Fig. 4. In the high-pressure flame the strong difference in signal strength in nonabsorbing environments persists; however, in the Diesel engine the signal strengths are all within the same order of magnitude. Longer-wavelength excitation should be

Table 3. Results of the Analysis for the Different Excitation and Detection Strategies: Calculated Transmission Properties of CO_2 and H_2O Exhaust for Two Practical Situations

NO *A–X* Band	(0, 0) Excitation (0, 1) + (0, 2) Detection	(0, 1) Excitation (0, 0) Detection	(0, 1) Excitation (0, 2) + (0, 3) Detection	(0, 2) Excitation (0, 0) + (0, 1) Detection	(0, 2) Excitation (0, 3) + (0, 4) Detection
Case 1: High-pressure burner, 40 bar, 1900 K					
Laser transmission, l = 4 mm	82%	89%	89%	95%	95%
Signal transmission, l = 4 mm	92%	81%	95%	87%	98%
Total transmission	75%	73%	85%	82%	92%
Relative overall NO LIF signal	75	11	24	2.5	1.2
Case 2: Diesel engine, 50 bar, 2400 K					
Laser transmission, l = 40 mm	0.48%	4.0%	4.0%	17%	17%
Signal transmission, l = 10 mm	53%	26%	67%	38%	80%
Total transmission	0.25%	1.0%	2.7%	6.4%	13%
Relative overall NO LIF signal	0.25	0.16	0.77	0.20	0.18

preferred here because the overall transmission is much larger and signals are therefore less influenced by fluctuations of pressure or temperature.

It is important to emphasize that the transmission properties strongly depend on the specific combustion situation (pressure, temperature) and experimental geometry (laser and signal paths). In IC engines, for example, signal transmission may increase, decrease, or stay constant with piston position (crank angle degree) because of the simultaneous variation of pressure, temperature, and path length, depending on the position of the laser beam above the piston window. The advantage of long-wavelength excitation is most pronounced at high pressure (above approximately 40 bar) and long laser path lengths.

C. Signal Interference

High-pressure NO LIF suffers from two types of interference: (i) narrowband in excitation and emission (O_2 LIF) and (ii) broadband in excitation and emission (CO_2 and PAH LIF). Although the choice of the vibrational bands used for excitation affects the broadband interference problems, the choice of a particular rotational absorption feature within the vibrational band is largely responsible for the contribution of narrowband O_2 LIF interference. The choice of the detection bandpass is important for efficient suppression of both kinds of interference.

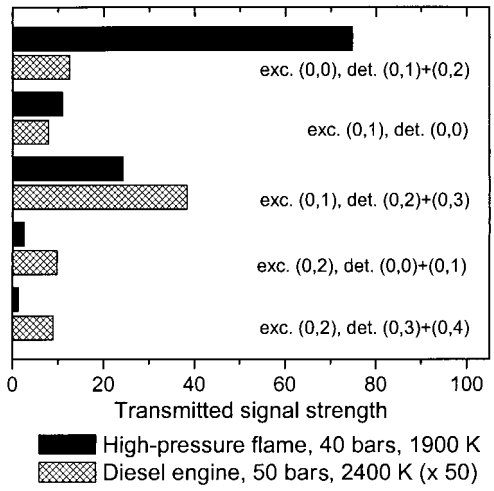

Fig. 4. Calculated signal strengths after laser and signal absorption by hot CO_2 and H_2O, normalized to the (0, 0) strategy signal without absorption for the Excited (exc.) and detected (det.) vibrational bands within the NO *A–X* system.

Figure 5 shows the contribution of interference to the LIF signal of 300-ppm NO for the different strategies for lean ($\phi = 0.83$) and rich ($\phi = 1.13$) flames with pressures between 1 and 60 bar; these results are also summarized in Table 4 for 10 and 60 bar. We quantified the LIF signal ratios O_2/NO and CO_2/NO as well as the LIF signal ratios of NO to the total emission (NO + O_2 + CO_2). This latter ratio is a measure for the spectral purity of the detected NO LIF signal. The interference strongly increases with pressure. NO emission gets weaker with increasing pressure because of pressure broadening leading to a decrease in excitation efficiency, whereas the effects of fluorescence quantum yield and NO number density cancel for constant mole fraction. O_2 and CO_2 emission increases linearly with pressure because of the increase in number density, whereas their fluorescence quantum yields stay approximately constant as is expected for excited electronic states with lifetimes limited by fast collision-independent processes (i.e., predissociation).

O_2 LIF is the main source of interference in lean flames. Note that all schemes were chosen to minimize O_2 absorption in the respective vibrational bands.[4,5] Still, its LIF contribution can reach the same order of magnitude as the NO signal in the lean 60-bar flame investigated here. The relative O_2 LIF interference increases in the order of (0, 0), (0, 1), and (0, 2) excitation. With (0, 1) excitation there is essentially no difference between red- or blue-shifted detection; with (0, 2) excitation, blue-shifted detection suppresses the O_2 LIF signal by a factor of 2 in comparison with red-shifted detection.

CO_2 LIF is important in both lean and rich flames,

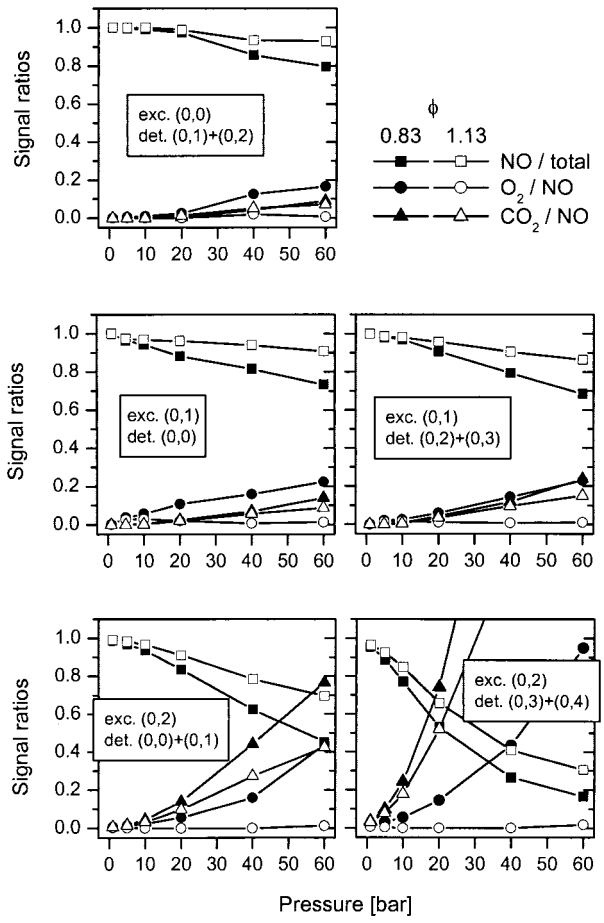

Fig. 5. Ratios of the LIF signal from 300-ppm NO and interference signals for different excitation (exc.) and detection (det.) strategies in lean and rich flames. Plotted are the LIF signal ratios NO/total (NO + O_2 + CO_2) as a measure of overall signal purity, and LIF signal ratios O_2/NO and CO_2/NO as a measure of interference signal strength. Excitation within the (0, 0), (0, 1), and (0, 2) bands is performed at 226.03, 235.87, and 247.94 nm, respectively.

especially if a broad detection bandpass is used. Its relative contribution is strongly increasing in the order of (0, 0) and (0, 1) excitation and is the dominant source of interference with (0, 2) excitation because the NO LIF intensity shows a stronger decrease with increasing excitation wavelength than the CO_2 LIF intensity. CO_2 LIF is generally much stronger with red-shifted detection in comparison with blue-shifted detection.

The signal purity (NO/total emission) is the most relevant parameter for a practical imaging application because it is the direct measure of how much of the detected signal is due to NO. From Fig. 5 it can be seen that it decreases almost linearly with pressure for all investigated strategies. It is also generally lower in lean flames than in rich flames because of both higher O_2 and CO_2 interference. The (0, 0) excitation strategy is the best choice for highest signal purities; (0, 1) strategies with both red- and blue-shifted detection yield only slightly lower purities. With (0, 2) excitation, blue-shifted detection shows a much better performance than red-shifted detection; still, signal purity may become as low as 50% in the lean 60-bar flame.

The discussion so far was based on the results of the seeded laminar high-pressure burner (LIF signal of 300-ppm NO). In IC engines, NO concentrations may be much higher (>1000 ppm), whereas in unseeded high-pressure burners NO concentration is often much lower (<100 ppm). The importance of signal interference therefore strongly depends on the particular combustion situation.

Note that the measurements in modestly rich ($\phi <$ 1.2) premixed flames avoid the potential PAH interference present in rich or nonpremixed combustion environments. The quantitative assessment of PAH interference is beyond the scope of this paper.

D. Temperature and Pressure Dependence

Quantitative NO concentration measurements without the exact knowledge of local temperature require us to choose a transition that minimizes the temperature sensitivity. The main temperature influence of NO LIF signal strength (on a per molecule basis) arises from the ground-state population of the laser-coupled levels. Because line broadening and shifting is temperature dependent, the overlap of the spectral features with the spectral shape of the laser also shows temperature dependence. Temperature furthermore influences the fluorescence quantum yield by changing collisional frequencies and quenching cross sections. The combined temperature effects of ground-state population, spectral overlap,

Table 4. Results of the Analysis for the Different Excitation and Detection Strategies: LIF Signal Interference Relative to the LIF Signal of 300-ppm NO at 10 Bar (60 Bar) (Percent)

NO *A–X* Band	(0, 0) Excitation (0, 1) + (0, 2) Detection	(0, 1) Excitation (0, 0) Detection	(0, 1) Excitation (0, 2) + (0, 3) Detection	(0, 2) Excitation (0, 0) + (0, 1) Detection	(0, 2) Excitation (0, 3) + (0, 4) Detection
O_2/NO ratio, ϕ = 0.83	0.9 (17)	5.7 (22)	2.4 (23)	2.3 (44)	5.5 (96)
CO_2/NO ratio, ϕ = 0.83	0 (8.9)	0.4 (14)	0.6 (24)	4.6 (77)	24 (412)
NO/(NO + O_2 + CO_2), ϕ = 0.83	99 (80)	94 (73)	97 (68)	94 (45)	77 (16)
O_2/NO ratio, ϕ = 1.13	0 (0.6)	3.0 (1.3)	1.6 (0.9)	0 (1.3)	0 (1.5)
CO_2/NO ratio, ϕ = 1.13	0 (7.0)	0.2 (8.8)	0.4 (15)	3.3 (42)	17 (222)
NO/(NO + O_2 + CO_2), ϕ = 1.13	99 (93)	94 (91)	97 (86)	94 (70)	77 (31)

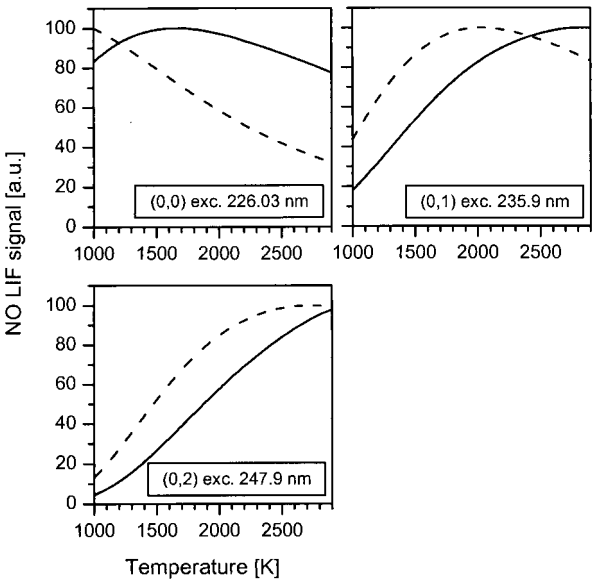

Fig. 6. Simulated temperature dependence of the NO LIF signal at fixed number densities or mole fractions. The simulations are performed for $p = 10$ bar, $T = 1900$ K, with the laser tuned to a constant excitation (exc.) wavelength corresponding to the NO peak at 10 bar. Solid curves, constant NO number density; dashed curves, constant NO mole fractions.

and quantum yield were calculated for the different strategies in the 10-bar flame with a 0.4-cm^{-1} laser FWHM based on a nontransient three-level NO LIF model.[4]

LIF signals are proportional to the local NO number density N_{NO} (in molecules per volume). In many combustion situations, not only the measurement of number density but the direct measurement of mole fractions $x_{NO} = N_{NO}/N_{total}$ is of interest, where $N_{total} = p/kT$ (ideal gas law). Thus

$$I_{LIF} \sim N_{NO} = x_{NO} * p/kT. \quad (1)$$

When mole fractions are evaluated from LIF intensities, the overall temperature sensitivity is altered because of the additional $1/T$ term. Typically this reduces the temperature sensitivity of hot transitions in the moderate temperature range and thus enables their use for quantitative measurements without temperature corrections.[4,73,75]

Figure 6 shows and compares the temperature sensitivity of LIF intensities for both fixed NO number density and fixed mole fractions. The data are also given in Table 5. For number density measurements, the LIF signal yield is relatively independent of temperature for A–X(0, 0) excitation strategies. Because of the large ground-state energies of A–X(0, 1) and (0, 2) transitions, the maximum LIF signal is found at high temperatures of 2815 K for the (0, 1) strategy and 3770 K for the (0, 2) strategy, and signals are strongly decreasing toward lower temperatures. Correction for this temperature effect is necessary for interpretation of the LIF signal when NO number densities are measured.

When mole fractions are measured, temperature sensitivity is most pronounced for (0, 0) excitation, where the signal continually decreases above 1000 K. With (0, 1) and (0, 2) excitation, the least temperature sensitivity is found around 2055 and 2715 K, respectively. Mole fractions are therefore best derived from experiments with (0, 1) or (0, 2) excitation for minimum temperature sensitivity.

Table 5 also gives the magnitude of the LIF signal variation between 1700 and 2500 K. This corresponds to the systematic error that is induced in NO concentration measurements in this temperature interval typical for high-pressure combustion situations when no temperature information is available for correction of the LIF signals. For number density measurements, the (0, 0) approach yields the least temperature variation of ±7% (relative to the average signal). For mole fraction measurements, the (0, 1) approach yields a temperature variation of only ±3%. If local temperature is not known, these strategies should be chosen to minimize systematic errors, depending on the choice of measured quantity.

The LIF signal depends on pressure through the change in excitation efficiency (line broadening and shifting) and fluorescence quantum yield (quench-

Table 5. Results of the Analysis for the Different Excitation and Detection Strategies: Simulated Temperature Dependence at 10 Bar

NO A–X Band	(0, 0) Excitation (0, 1) + (0, 2) Detection	(0, 1) Excitation; either (0, 0) or (0, 2) + (0, 3) Detection	(0, 2) Excitation; either (0, 0) + (0, 1) or (0, 3) + (0, 4) Detection
Temperature of maximum LIF signal, number density measurement	1645 K	2815 K	3770 K
Signal variation between 1700 and 2500 K, number density measurement	± 6.8%	± 18%	± 36%
Temperature of maximum LIF signal, mole fraction measurement	<1000 K	2055 K	2715 K
Signal variation between 1500 and 2500 K, mole fraction measurement	± 25%	± 3.1%	± 19%

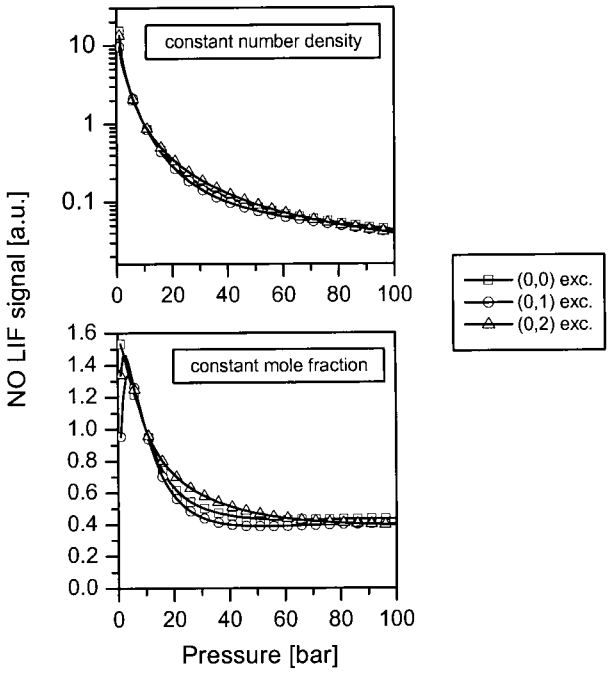

Fig. 7. Simulated pressure dependence of the NO LIF signal for number density and mole fraction measurement, normalized to the 10-bar value. The laser is tuned to a constant excitation (exc.) wavelength corresponding to the NO peak at 10 bar. Note the different scales (logarithmic and linear) in the two panels.

ing). The overall effect leads to a strong nonlinear decrease in LIF signal with pressure. The simulated pressure dependence of the NO LIF signal for constant number density (corresponding to the signal strength on a per molecule base) is shown in the upper panel of Fig. 7 for the three excitation strategies. The LIF signal strength decreases by more than 2 orders of magnitude between 1 and 40 bar. In practice this decrease is partly compensated by the effect of an increasing number density with pressure, leading to strong LIF signals even at elevated pressures.

When LIF measurements are performed to quantify mole fractions, quenching (which is $\sim p$ and therefore decreases the fluorescence quantum yield $\sim 1/p$) cancels with the pressure dependence of the number density [which is $\sim p$, see Eq. (1)]. The variation of signal with pressure then depends only on the pressure-dependent spectral overlap between laser and absorption feature. The resulting simulated signal strengths are shown in the lower panel of Fig. 7. These data correspond to the pressure dependence of the overlap fraction, i.e., the absorption efficiency.

Because of the particular shape of the absorption feature and the density of transitions nearby, the pressure dependence varies slightly for the different excitation approaches. It is interesting to note that above approximately 50 bar, absorption efficiency does not change any more; instead, all rotational lines of the vibrational band are completely merged by pressure broadening. Because pressure is readily measured in most static and fluctuating combustion situations, we can relatively easily account for the pressure effects.

5. Conclusions

We compared five practical schemes for NO A–X LIF, which involve exciting transitions in the (0, 0), (0, 1), and (0, 2) bands and the detection of red- and blue-shifted wavelengths relative to the excitation wavelength. No single best strategy can be suggested for all combustion situations. The choice is a trade-off between selectivity and signal intensity and the optical accessibility in terms of laser and signal absorption. The properties of the five strategies compared in this paper are summarized as follows:

- The (0, 0) approach (excitation at 226.03 nm, only red-shifted detection is possible) clearly offers the best performance in terms of signal strength and selectivity. It is the strategy of choice for combustion diagnostics at all pressures as long as laser attenuation is acceptably low. It is therefore especially suitable for high-pressure combustion with small flame diameters. The temperature sensitivity allows measurement of NO number densities even without detailed knowledge of local temperatures. However, at high pressures and temperatures (>40 bar, >2200 K), especially in IC engines, laser attenuation may reach levels that make quantitative or even qualitative measurements impossible with the (0, 0) excitation strategy. The red-shifted detection of potential PAH interference may further complicate this approach.
- The (0, 1) approach (excitation at 235.87 nm) with red-shifted detection is attractive, although it has scarcely been applied. It offers relatively strong signals [approximately one third of the (0, 0) approach] and at the same time reduces attenuation of both laser and signal light, especially if the experiment requires long signal paths. Signal purity is still good at intermediate NO concentrations (around 300 ppm). The temperature sensitivity allows measurement of NO mole fractions even without detailed knowledge of local temperatures. However, this red-shifted detection scheme may allow unwanted PAH interference.
- Blue-shifted detection after (0, 1) excitation offers no particular advantage in signal strength, signal purity, or transmission properties. This might change in the presence of PAH.
- The (0, 2) approach (excitation at 247.94 nm) with blue-shifted detection has been widely employed in high-pressure high-temperature combustion situations. Although the signal strength is low, it strongly reduces attenuation problems in typical in-cylinder experimental geometries with long laser path and short signal path. Interference levels are acceptable for high NO concentrations (>1000 ppm). In addition, previous literature suggests that this approach is most effective to minimizing PAH interference.

• Excitation within the (0, 2) band with red-shifted detection suffers both in signal strength and in interference and is not recommended.

Our research at Stanford University is supported by the U.S. Air Force Office of Scientific Research, Aerospace Sciences Directorate, with Julian Tishkoff as the technical monitor. The Division of International Programs at the National Science Foundation supports the Stanford collaboration through a cooperative research grant. The University of Heidelberg research and the travel of W. G. Bessler and C. Schulz are sponsored by the Deutsche Forschungsgemeinschaft and the Deutsche Akademische Auslandsdienst.

References

1. A. C. Eckbreth, *Laser Diagnostics for Combustion Temperature and Species*, 2nd ed. (Gordon and Breach, Amsterdam, The Netherlands, 1996).
2. K. Kohse-Höinghaus, "Laser techniques for the quantitative detection of reactive intermediates in combustion systems," Prog. Energy Combust. Sci. **20,** 203–279 (1994).
3. K. Kohse-Höinghaus and J. B. Jeffries, *Applied Combustion Diagnostics* (Taylor & Francis, New York, 2002).
4. W. G. Bessler, C. Schulz, T. Lee, J. B. Jeffries, and R. K. Hanson, "Strategies for laser-induced fluorescence detection of nitric oxide in high-pressure flames. I. *A–X*(0, 0) excitation," Appl. Opt. **41,** 3547–3557 (2002).
5. W. G. Bessler, C. Schulz, T. Lee, J. B. Jeffries, and R. K. Hanson, "Strategies for laser-induced fluorescence detection of nitric oxide in high-pressure flames. II. *A–X*(0, 1) excitation," Appl. Opt. **42,** 2031–2042 (2003).
6. C. Schulz, V. Sick, J. Heinze, and W. Stricker, "Laser-induced fluorescence detection of nitric oxide in high-pressure flames with *A–X*(0, 2) excitation," Appl. Opt. **36,** 3227–3232 (1997).
7. C. Schulz, V. Sick, U. Meier, J. Heinze, and W. Stricker, "Quantification of NO *A–X*(0, 2) laser-induced fluorescence: investigation of calibration and collisional influences in high-pressure flames," Appl. Opt. **38,** 1434–1443 (1999).
8. A. Y. Chang, M. D. DiRosa, and R. K. Hanson, "Temperature dependence of collision broadening and shift in the NO A–X(0, 0) band in the presence of argon and nitrogen," J. Quant. Spectrosc. Radiat. Transfer **47,** 375–390 (1992).
9. M. D. DiRosa and R. K. Hanson, "Collision broadening and shift of NO (0, 0) absorption lines by O_2 and H_2O at high temperatures," J. Quant. Spectrosc. Radiat. Transfer **52,** 515–529 (1994).
10. M. D. DiRosa and R. K. Hanson, "Collision-broadening and -shift of NO (0, 0) absorption lines by H_2O, O_2 and NO at 295 K," J. Mol. Spectrosc. **164,** 97–117 (1994).
11. A. O. Vyrodov, J. Heinze, and U. E. Meier, "Collisional broadening of spectral lines in the A-X(0, 0) system of NO by N_2, Ar, and He at elevated pressures measured by laser-induced fluorescence," J. Quant. Spectrosc. Radiat. Transfer **53,** 277–287 (1995).
12. R. Zhang and D. R. Crosley, "Temperature dependent quenching of A $^2\Sigma^+$ NO between 215 and 300 K," J. Chem. Phys. **102,** 7418–7424 (1995).
13. P. H. Paul, J. A. Gray, J. L. Durant, Jr., and J. W. Thoman, Jr., "Collisional electronic quenching rates for NO $A^2\Sigma^+$ ($v' = 0$)," Chem. Phys. Lett. **259,** 508–541 (1996).
14. M. C. Drake and J. W. Ratcliffe, "High temperature quenching cross sections for nitric oxide laser-induced fluorescence measurements," J. Chem. Phys. **98,** 3850–3865 (1993).
15. J. W. Thoman, J. A. Gray, J. L. Durant, and P. H. Paul, "Collisional electronic quenching of NO $A^2\Sigma^+$ by N_2 from 300 to 4500 K," J. Chem. Phys. **97,** 8156–8163 (1992).
16. P. H. Paul, J. A. Gray, J. L. Durant, Jr., and J. W. Thoman, Jr., "A model for temperature-dependent collisional quenching of NO $A^2\Sigma^+$," Appl. Phys. B **57,** 249–259 (1993).
17. M. Tamura, P. A. Berg, J. E. Harrington, J. Luque, J. B. Jeffries, G. P. Smith, and D. R. Crosley, "Collisional quenching of CH (A), OH A, and NO (A) in low-pressure hydrocarbon flames," Combust. Flame **114,** 502–514 (1998).
18. P. H. Paul, C. D. Carter, J. A. Gray, J. L. Durant, Jr., J. W. Thoman, and M. R. Furlanetto, "Correlations for the NO $A^2\Sigma^+$ ($v' = 0$) electronic quencing cross-section," Sandia Rep. SAND94–8237 UC-1423 (Sandia National Laboratories, Livermore, Calif., 1994).
19. R. S. Barlow and J. H. Frank, "Effects of turbulence on species mass fractions in methane/air jet flames," Proc. Combust. Inst. **27,** 1087–1095 (1998).
20. F. Hildenbrand and C. Schulz, "Measurements and simulation of in-cylinder UV-absorption in spark ignition and Diesel engines," Appl. Phys. B **73,** 165–172 (2001).
21. C. Schulz, J. D. Koch, D. F. Davidson, J. B. Jeffries, and R. K. Hanson, "Ultraviolet absorption spectra of shock-heated carbon dioxide and water between 900 and 3050 K," Chem. Phys. Lett. **355,** 82–88 (2002).
22. W. G. Bessler, C. Schulz, T. Lee, D. I. Shin, M. Hofmann, J. B. Jeffries, J. Wolfrum, and R. K. Hanson, "Quantitative NO-LIF imaging in high-pressure flames," Appl. Phys. B **75,** 97–102 (2002).
23. C. Schulz, J. B. Jeffries, D. F. Davidson, J. D. Koch, J. Wolfrum, and R. K. Hanson, "Impact of UV absorption by CO_2 and H_2O on NO LIF in high-pressure combustion applications," Proc. Combust. Inst. **29,** 2725–2743 (2002).
24. M. D. DiRosa, K. G. Klavuhn, and R. K. Hanson, "LIF Spectroscopy of NO and O_2 in high-pressure flames," Combust. Sci. Technol. **118,** 257–283 (1996).
25. W. G. Bessler, C. Schulz, T. Lee, J. B. Jeffries, and R. K. Hanson, "Carbon dioxide UV laser-induced fluorescence in high-pressure flames," Chem. Phys. Lett. **375,** 344–349 (2003).
26. A. Cialolo, R. Barbella, A. Tregrossi, and L. Bonfanti, "Spectroscopic and compositional signatures of PAH-loaded mixtures in the soot inception region of a premixed ethylene flame," Proc. Combust. Inst. **27,** 1481–1487 (1998).
27. P.-E. Bengtsson and M. Aldén, "Soot-visualization strategies using laser techniques," Appl. Phys. B **60,** 51–59 (1995).
28. M. Hofmann, W. G. Bessler, C. Schulz, and H. Jander, "Laser-induced incandescence for soot diagnostics at high pressure," Appl. Opt., **425** 2052–2062 (2003).
29. A. M. Wodtke, M. Huwel, H. Schluter, G. Meijer, P. Andresen, and H. Voges, "High-sensitivity detection of NO in a flame using a tunable ArF laser," Opt. Lett. **13,** 910–912 (1988).
30. M. Versluis, M. Ebben, M. Drabbels, and J. J. ter Meulen, "Frequency calibration in the ArF excimer laser-tuning range using laser-induced fluorescence of NO," Appl. Opt. **30,** 5229–5234 (1991).
31. P. Andresen, G. Meijer, H. Schluter, H. Voges, A. Koch, W. Hentschel, W. Oppermann, and E. Rothe, "Fluorescence imaging inside an internal combustion engine using tunable excimer lasers," Appl. Opt. **29,** 2392–2404 (1990).
32. A. Arnold, F. Dinkelacker, T. Heitzmann, P. Monkhouse, M. Schäfer, V. Sick, J. Wolfrum, W. Hentschel, and K.-P. Schindler, "DI Diesel engine combustion visualized by combined laser techniques," Proc. Combust. Inst. **24,** 1605–1612 (1992).
33. A. Arnold, A. Bräumer, A. Buschmann, M. Decker, F. Dinkelacker, T. Heitzmann, A. Orth, M. Schäfer, V. Sick, and J. Wolfrum, "2D-diagnostics in industrial devices," Ber. Bunsenges. Phys. Chem **97,** 1650–1661 (1993).
34. T. M. Brugmann, R. Klein-Douwel, G. Huigen, E. van Walwijk, and J. J. ter Meulen, "Laser-induced-fluorescence imaging of

NO in an n-heptane- and Diesel-fuel-driven Diesel engine," Appl. Phys. B **57,** 405–410 (1993).
35. T. M. Brugmann, G. G. M. Stoffels, N. Dam, W. L. Meerts, and J. J. t. Meulen, "Imaging and post-processing of laser-induced fluorescence from NO in a Diesel engine," Appl. Phys. B **64,** 717–724 (1997).
36. N. Dam, W. L. Meerts, and J. J. ter Meulen, "Laser diagnostics of nitric oxide inside a two-stroke DI Diesel engine," in *Laser Techniques Applied to Fluid Mechanics*: *Selected Papers from the Ninth International Symposium*, R. J. Adrian, D. F. G. Durao, F. Durst, M. V. Heitor, M. Maeda, and J. H. Whitelaw, eds. (Springer-Verlag, New York, 2000), chap. 7.
37. G. G. M. Stoffels, E.-J. van den Boom, C. M. I. Spaanjaars, N. Dam, W. L. Meerts, J. J. ter Meulen, J. L. C. Duff, and D. J. Rickeard, "In-cylinder measurements of NO formation in a Disel engine," SAE Tech. Paper Series, 1999-01-1487 (Society of Automotive Engineers, Warrendale, Pa., 1999).
38. T. Tanaka, M. Fujimoto, and M. Tabata, "Planar measurements of NO in an S.I. engine based on laser induced fluorescence," SAE Tech. Paper Series, 970877 (Society of Automotive Engineers, Warrendale, Pa., 1997).
39. B. K. McMillin, J. L. Palmer, and R. K. Hanson, "Temporally resolved, two-line fluorescence imaging of NO temperature in a transverse jet in a supersonic cross flow," Appl. Opt. **32,** 7532–7545 (1993).
40. J. L. Palmer and R. K. Hanson, "Shock tunnel flow visualization using planar laser-induced fluorescence imaging of NO and OH," Shock Waves **4,** 313–323 (1995).
41. D. D. Thomsen, F. F. Kuligowski, and N. M. Laurendeau, "Modeling of NO formation in premixed, high-pressure methane flames," Combust. Flame **119,** 307–318 (1999).
42. J. E. Dec and R. E. Canaan, "PLIF imaging of NO formation in a DI Diesel engine," SAE Tech. Paper Series, 980147 (Society of Automotive Engineers, Warrendale, Pa., 1998).
43. B. Alatas, J. A. Pinson, T. A. Litzinger, and D. A. Santavicca, "A study of NO and soot evolution in a DI Diesel engine via planar imaging," SAE Tech. Paper Series 930973 (Society of Automotive Engineers, Warrendale, Pa., 1993).
44. A. Bräumer, V. Sick, J. Wolfrum, V. Drewes, M. Zahn, and R. Maly, "Quantitative two-dimensional measurements of nitric oxide and temperature distributions in a transparent square piston SI engine," SAE Tech. Paper Series, 952462 (Society of Automotive Engineers, Warrendale, Pa., 1995).
45. T. Dreier, A. Dreizler, and J. Wolfrum, "The application of a Raman-shifted tunable KrF excimer laser for laser-induced fluorescence combustion diagnostics," Appl. Phys. B **55,** 381–387 (1992).
46. B. E. Battles and R. K. Hanson, "Laser-induced fluorescence measurements of NO and OH mole fraction in fuel-lean, high-pressure (1–10 atm) methane flames: fluorescence modeling and experimental validation," J. Quant. Spectrosc. Radiat. Transfer **54,** 521–537 (1995).
47. E.-J. van den Boom, P. B. Monkhouse, C. M. I. Spaanjaars, W. L. Meerts, N. J. Dam, and J. J. ter Meulen. "Laser diagnostics in a Diesel engine," in *ROMOPTO 2000: Sixth Conference on Optics*, V. I. Vlad, ed., Proc. SPIE **4430,** 593–600 (2001).
48. H. Nakagawa, H. Endo, Y. Deguchi, M. Noda, H. Oikawa, and T. Shimada, "NO measurement in Diesel spray flame using laser induced fluorescence," SAE Tech. Paper Series 970874 (Society of Automotive Engineers, Warrendale, Pa., 1997).
49. M. C. Drake, J. W. Ratcliffe, R. J. Blint, C. D. Carter, and N. M. Laurendeau, "Measurements and modeling of flamefront NO formation and superequilibrium radical concentrations in laminar high-pressure premixed flames," Proc. Combust. Inst. **23,** 387–395 (1990).
50. J. R. Reisel, C. D. Carter, and N. M. Laurendeau, "Laser-induced fluorescence measurements of nitric oxide in laminar $C_2H_6/O_2/N_2$ flames at high pressure," Combust. Flame **92,** 485–489 (1993).
51. J. R. Reisel and N. M. Laurendeau, "Laser-induced fluorescence measurements and modeling nitric oxide formation in high-pressure flames," Combust. Sci. Technol. **98,** 137–160 (1994).
52. J. R. Reisel and N. M. Laurendeau, "Quantitative LIF measurements of nitric oxide in laminar high-temperature flames," Energy Fuels **8,** 1115–1122 (1994).
53. J. R. Reisel and N. M. Laurendeau, "Quantitative LIF measurements and modeling of nitric oxide in high-pressure $C_2H_4/O_2/N_2$ flames," Combust. Flame **101,** 141–152 (1995).
54. C. S. Cooper and N. M. Laurendeau, "Parametric study of NO production via quantitative laser-induced fluorescence in high-pressure, swirl-stabilized spray flames," Proc. Combust. Inst. **28,** 287–293 (2000).
55. C. S. Cooper and N. M. Laurendeau, "Comparison of laser-induced and planar laser-induced fluorescence measurements of nitric oxide in a high-pressure, swirl-stabilized, spray flame," Appl. Phys. B **70,** 903–910 (2000).
56. C. S. Cooper and N. M. Laurendeau, "Quantitative measurements of nitric oxide in high-pressure (2–5 atm), swirl-stabilized spray flames via laser-induced fluorescence," Combust. Flame **123,** 175–188 (2000).
57. D. Charlston-Goch, B. L. Chadwick, R. J. S. Morrison, A. Campisi, D. D. Thomsen, and N. M. Laurendeau, "Laser-induced fluorescence measurements and modeling of nitric oxide in premixed flames of $CO+H_2+CH_4$ and air at high pressures," Combust. Flame **125,** 729–743 (2001).
58. D. D. Thomsen, F. F. Kuligowski, and N. M. Laurendeau, "Background corrections for laser-induced-fluorescence measurements of nitric oxide in lean, high-pressure, premixed methane flames," Appl. Opt. **36,** 3244–3252 (1997).
59. W. P. Partridge, Jr. and N. M. Laurendeau, "Formulation of a dimensionless overlap fraction to account for spectrally distributed interactions in fluorescence studies," Appl. Opt. **34,** 2645–2647 (1995).
60. J. R. Reisel, W. P. Partridge, Jr., and N. M. Laurendeau, "Transportability of a laser-induced fluorescence calibration for NO at high pressure," J. Quant. Spectrosc. Radiat. Transfer **53,** 165–178 (1995).
61. C. S. Cooper and N. M. Laurendeau, "Laser-induced fluorescence measurements in lean direct-injection spray flames: technique development and application," Meas. Sci. Technol. **11,** 902–911 (2000).
62. W. G. Bessler, C. Schulz, T. Lee, D. I. Shin, M. Hofmann, J. B. Jeffries, J. Wolfrum, and R. K. Hanson. "Quantitative NO-LIF imaging in high-pressure flames," in *First International Conference on Optical and Laser Diagnostics* (*ICOLAD*) (Institute of Physics, London, 2002), pp. 97–102.
63. A. O. Vyrodov, J. Heinze, M. Dillmann, U. E. Meier, and W. Stricker, "Laser-induced fluorescence thermometry and concentration measurements on NO A-X(0, 0) transitions in the exhaust gas of high pressure CH_4/air flames," Appl. Phys. B. **61,** 409–414 (1995).
64. P. Jamette, P. Desgroux, V. Ricordeau, and B. Deschamps, "Laser-induced fluorescence detection of NO in the combustion chamber of an optical GDI engine with A-X(0, 1) excitation," SAE Tech. Paper Series 2001-01-1926 (Society of Automotive Engineers, Warrendale, Pa., 2001).
65. W. G. Bessler, C. Schulz, T. Lee, J. B. Jeffries, and R. K. Hanson. "Laser-induced-fluorescence detection of nitric oxide in high-pressure flames with A-X(0, 1) excitation," in *Proceedings of the Western States Section of the Combustion Institute, Spring Meeting* (Combustion Institute, Pittsburgh, Pa., 2001).
66. T. Lee, D.-I. Shin, J. B. Jeffries, R. K. Hanson, W. G. Bessler, and C. Schulz, "Laser-induced fluorescence detection of NO in methane/air flames at pressures between 1 and 60 bar," paper

AIAA-2002-0399, presented at the Fortieth Aerospace Sciences Meeting and Exhibit, Reno, Nev., 5–8 Jan. 2002 (American Institute of Aeronautics and Astronautics, Reston, Va., 2002).
67. C. Schulz, B. Yip, V. Sick, and J. Wolfrum, "A laser-induced fluorescence scheme for imaging nitric oxide in engines," Chem. Phys. Lett. **242,** 259–264 (1995).
68. C. Schulz, V. Sick, J. Heinze, and W. Stricker, "A new approach to laser-induced fluorescence detection of nitric oxide in high pressure flames," in *Laser Applications to Chemical, Biological and Environmental Analysis*, Vol. 3. of 1996 OSA Technical Digest Series (Optical Society of America, Washington, D.C., 1996), pp. 133–135.
69. F. Hildenbrand, C. Schulz, M. Hartmann, F. Puchner, and G. Wawrschin, "In-cylinder NO-LIF imaging in a realistic GDI engine using KrF excimer laser excitation," SAE Tech. Paper Series 1999-01-3545 (Society of Automotive Engineers, Warrendale, Pa., 1999).
70. F. Hildenbrand, C. Schulz, V. Sick, H. Jander, and H. G. Wagner, "Applicability of KrF excimer laser induced fluorescence in sooting high-pressure flames," in VDI Flammentag Dresden, VDI Berichte 1492 (1999), pp. 269–274.
71. F. Hildenbrand, C. Schulz, V. Sick, and E. Wagner, "Spatially resolved investigation of light absorption in an SI engine fueled with propane/air," Appl. Opt. **38,** 1452–1458 (1999).
72. C. Schulz, V. Sick, J. Wolfrum, V. Drewes, M. Zahn, and R. Maly, "Quantitative 2D single-shot imaging of NO concentrations and temperatures in a transparent SI engine," Proc. Combust. Inst. **26,** 2597–2604 (1996).
73. W. G. Bessler, C. Schulz, M. Hartmann, and M. Schenk, "Quantitative in-cylinder NO-LIF imaging in a direct-injected gasoline engine with exhaust gas recirculation," SAE Tech. Paper Series 2001-01-1978 (Society of Automotive Engineers, Warrendale, Pa., 2001).
74. F. Hildenbrand, C. Schulz, J. Wolfrum, F. Keller, and E. Wagner, "Laser diagnostic analysis of NO formation in a direct injection Diesel engine with pump-line nozzle and common-rail injection systems," Proc. Combust. Inst. **28,** 1137–1144 (2000).
75. F. Hildenbrand, C. Schulz, F. Keller, G. König, and E. Wagner, "Quantitative laser diagnostic studies of the NO distribution in a DI Diesel engine with PLN and CR injection systems," SAE Tech. Paper 2001-01-3500 (Society of Automotive Engineers, Warrendale, Pa., 2001).
76. V. Beushàusen, M. Knapp, A. Luczak, S. Eisenberg, and P. Andresen, "Application of laser-induced fluorescence and spontaneous Raman scattering to technically applied combustion systems: four cylinder spark ignition engine and oil burning furnace," in *Laser Applications to Chemical, Biological and Environmental Analysis*, Vol. 3 of 1996 OSA Technical Digest Series (Optical Society of America, Washington, D.C., 1996), pp. 142–144.
77. M. Knapp, A. Luczak, H. Schlüter, V. Beushausen, W. Hentschel, and P. Andresen, "Crank-angle-resolved laser-induced fluorescence imaging of NO in a spark-ignition engine at 248 nm and correlations to flame front propagation and pressure release," Appl. Opt. **35,** 4009–4017 (1996).
78. M. Knapp, A. Luczak, V. Beushausen, W. Hentschel, P. Manz, and P. Andresen, "Quantitative in-cylinder NO LIF measurements with a KrF excimer laser applied to a mass-production SI engine fueled with isooctane and regular gasoline," SAE Tech. Paper Series 970824 (Society of Automotive Engineers, Warrendale, Pa., 1997).
79. K. Akihama, T. Fujikawa, and Y. Hattori, "Laser-induced fluorescence imaging of NO in a port-fuel-injected statified-charge SI engine—correlations between NO formation region and stratified fuel distribution," SAE Tech. Paper Series 981430 (Society of Automotive Engineers, Warrendale, Pa., 1998).
80. H. Eberius, T. Just, T. Kick, G. Höfner, and W. Lutz. "Stabilization of premixed, laminar methane flames in the pressure regime up to 40 bar," in *Proceedings of the Joint Meeting German/Italian Section of the Combustion Institute* (Combustion Institute, Pittsburgh, Pa., 1989).
81. W. G. Bessler, C. Schulz, V. Sick, and J. W. Daily. "A versatile modeling tool for nitric oxide LIF spectra," in the *Third Joint Meeting of the U.S. Sections of the Combustion Institute* (Combustion Institute, Pittsburgh, Pa., 2003), p. P11–6.
82. A. V. Mokhov, H. B. Levinsky, and C. E. van der Meij, "Temperature dependence of laser-induced fluorescence of nitric oxide in laminar premixed atmospheric-pressure flames," Appl. Opt. **36,** 3233–3243 (1997).
83. P. H. Paul, "Calculation of transition frequencies and roational line strengths in the γ-bands of nitric oxide," J. Quant. Spectrosc. Radiat. Transfer **57,** 581–589 (1997).